NANO LETTERS

pubs.acs.org/NanoLett

Formation of Metastable Liquid Catalyst during Subeutectic Growth of Germanium Nanowires

A. D. Gamalski,[†] J. Tersoff,[‡] R. Sharma,[§,⊥] C. Ducati,[∥] and S. Hofmann*[,†]

[†]Department of Engineering, University of Cambridge, Cambridge CB3 0FA, U.K., [‡]IBM T.J. Watson Research Center, Yorktown Heights, New York 10598, [§]Center for Solid State Science, Arizona State University, Tempe, Arizona 85287-1704, and [∥]Department of Materials Science and Metallurgy, University of Cambridge, Cambridge CB2 3QZ, U.K.

ABSTRACT Lattice-resolved, video-rate environmental transmission electron microscopy shows the formation of a liquid Au−Ge layer on sub-30-nm Au catalyst crystals and the transition of this two-phase Au−Ge/Au coexistence to a completely liquid Au−Ge droplet during isothermal digermane exposure at temperatures far below the bulk Au−Ge eutectic temperature. Upon Ge crystal nucleation and subsequent Ge nanowire growth, the catalyst either recrystallizes or remains liquid, apparently stabilized by the Ge supersaturation. We argue that there is a large energy barrier to nucleate diamond-cubic Ge, but not to nucleate the Au−Ge liquid. As a result, the system follows the more kinetically accessible path, forming a liquid even at 240 °C, although there is no liquid along the most thermodynamically favorable path below 360 °C.

KEYWORDS Ge nanowire, nanocatalyst, CVD, phase-diagram, environmental TEM

The self-organized bottom-up growth of semiconductor nanowires (NWs) offers the prospect of device engineering at the nanoscale for applications in nanoelectronics, photonics, and sensors.[1−3] However, at the low processing temperatures desired for technology, there remain fundamental questions regarding the competing thermodynamic and kinetic factors - even whether the catalyst is solid or liquid for widely used semiconductor/catalyst systems such as Ge/Au,[4,5] Si/Al,[6,7] and GaAs/Au.[8,9] The physical and chemical state of the catalyst is of key importance to NW growth kinetics, orientation, and interface sharpness in NW heterostructures,[10] since it determines how quickly the chemical potential of the growth species can be raised to overcome nucleation barriers for NW and interfacial ledge formation.[11]

Ge/Au is an ideal system to explore these issues. There have been numerous reports of Au-catalyzed Ge NW chemical vapor deposition (CVD) with high growth rates at temperatures as low as 250 °C.[4,5,12−19] However, in most cases the experimental procedure involves a high temperature pretreatment, i.e., heating to above the Au−Ge bulk eutectic temperature $T_e = 361$ °C, to obtain a liquid Au−Ge catalyst alloy, which subsequently can be undercooled in the presence of (di)germane.[4,5] Such a process does not capture the full technological advantages of low-temperature processing. The only previous isothermal studies relied on postgrowth, ex situ analysis,[14,16] which allows only indirect inference regarding the initial stages of growth and the state of the catalyst. On the theoretical side, there have been many studies suggesting that nanoscale size effects could stabilize a liquid below T_e, but little work demonstrating such size effects under actual growth conditions.[5,20−22]

Here we use environmental transmission electron microscopy (ETEM) to achieve a lattice-resolved, video-rate record of sub-30-nm Au nanoparticles *during* isothermal digermane exposure at a temperature range of 240−280 °C. We show that our catalyst particles completely liquefy during Ge crystal nucleation at temperatures more than 100 °C below T_e and that kinetically driven supersaturations determine the catalyst phase during subsequent Ge NW growth. We propose that this behavior can be understood in terms of bulk thermodynamics, together with the radically different nucleation kinetics for liquid Au−Ge versus diamond-cubic (DC) Ge. Nanoscale size effects may also be important,[5,21,22] but they are not needed to account for low-T liquefaction.

Figure 1 shows the evolution of a Au catalyst particle on SiO_x support at ∼240 °C in ∼1.4×10^{-3} mbar Ge_2H_6. We use a modified Tecnai F20 ETEM, operated at 200 kV, equipped with a differential pumping system and a Gatan imaging filter. The microscope permits pressures of up to 10 mbar, with an information limit of 0.134 nm. Digital video sequences can be recorded with 15 frames/s time resolution using a Gatan Orius 600 camera. Temperatures are measured by a thermocouple on the TEM holder minifurnace. The electron dose was representative of that typically implemented for high-resolution imaging, and the electron beam was never focused onto the specimen in

* To whom correspondence should be addressed, sh315@cam.ac.uk.

⊥ Current address: National Institute of Standards and Technology, 100 Bureau Dr., Gaithersburg, MD 20899.

Received for review: 04/16/2010
Published on Web: 07/07/2010

DOI: 10.1021/nl101349e | *Nano Lett.* **2010,** *10,* 2972–2976

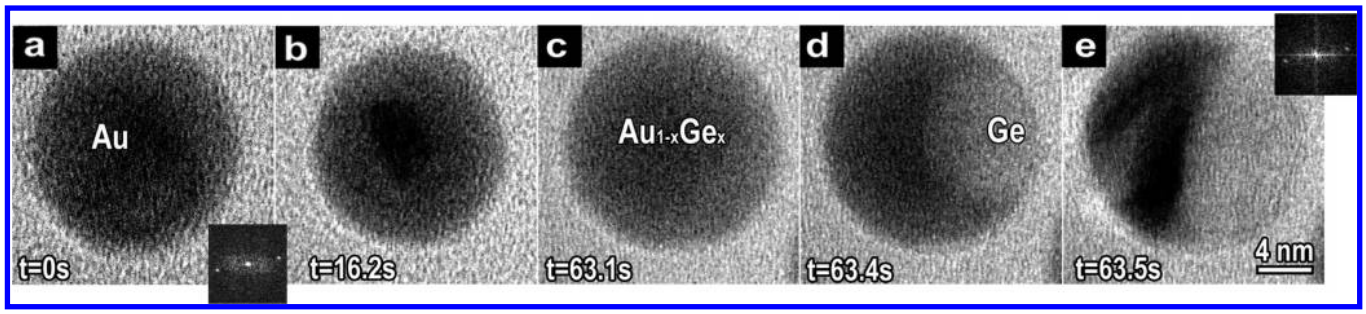

FIGURE 1. Bright-field ETEM image sequence of a Au catalyst particle on SiO_x support at ~240 °C exposed to ~1.4×10^{-3} mbar Ge_2H_6 (extracted from video S1, Supporting Information). The insets show fast Fourier transforms (FFTs) of the solid catalyst in frames a and e.

order to minimize the effects of electron-beam-induced damage/gas dissociation[23] and modification of the specimen.[24] The Au catalyst was prepared by thermal evaporation (nominal Au thickness <2 nm) onto perforated SiO_2 membranes (SPI supplies) or onto 2000 mesh Cu TEM grids coated with a holey carbon film (Agar Scientific) and a ~30 nm sputtered SiO_x layer. The samples were transferred in air to the ETEM. Unless stated otherwise, we use undiluted Ge_2H_6.

The Au particles are crystalline prior to Ge_2H_6 exposure. As digermane dissociates on their surfaces, a liquid Au−Ge layer immediately forms and wets the solid Au core of the particles (Figure 1a). The 0.23 nm reflection of the solid core (inset Figure 1a) can be assigned to {111} lattice planes in face-centered cubic (fcc) Au. Following the initial rapid liquefaction of the surface, the liquid Au−Ge phase front slows down while propagating radially inward and we observe a coexistence with a solid Au core for several tens of seconds, Figure 1b. Below a critical size, the solid Au core starts to shrink rapidly and abruptly disappears. This destabilization originates in the increasing chemical potential of the solid Au as it shrinks, analogous to the Gibbs−Thomson pressure.[22] After the disappearance of the solid Au core, the particle is entirely liquid, Figure 1c. The particle remains completely liquid for tens of seconds before DC Ge nucleates at the surface of the droplet (Figure 1d). Upon Ge nucleation, the liquid rapidly separates into two solid phases, apparently DC Ge and fcc Au (Figure 1e). The catalyst shows a fringe spacing of 0.21−0.22 nm at this stage (inset Figure 1e), which is consistent with fcc Au, given the possible imaging distortions and measurement uncertainties for the nanocrystals.

Until the nucleation of DC Ge, the evolution is similar to what has been reported for the Au−Si system *above* T_e—initial wetting with the eutectic liquid, with gradual shrinking of the fcc Au particle ending in an abrupt dissolution.[22] Yet our Au−Ge system is actually far *below* T_e. There has been much interest in the possibility that the liquid is thermodynamically stabilized by nanoscale size effects.[5,20,25] Here, we propose that the behavior can be explained by considering the kinetic competition between forming Au−Ge liquid vs DC Ge, even if size effects are not significant.

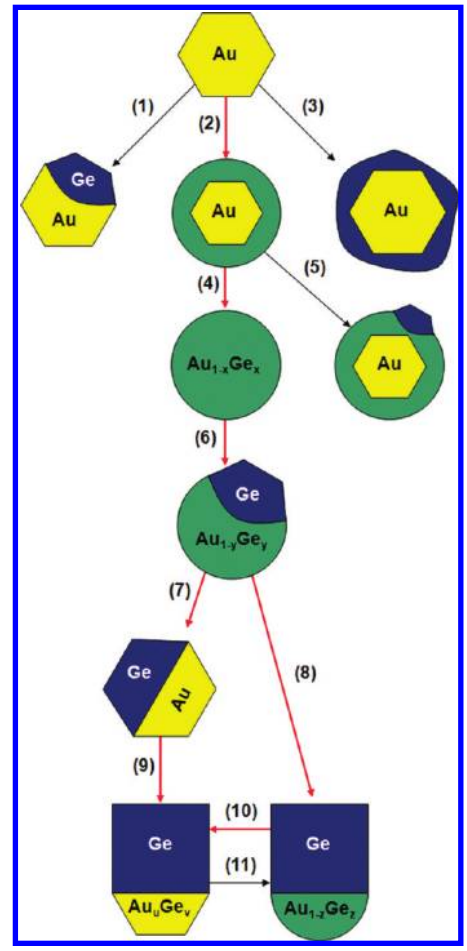

FIGURE 2. Schematic flowchart of potential processes for Ge_2H_6 exposed nanoparticulate Au. Observed processes are highlighted in red, whereby Figures 1 and 5a−d reflect sequences (2)−(4)−(6)−(7) and (2)−(4)−(6)−(8), respectively.

Figure 2 shows a schematic flowchart of potential processes for the Au−Ge system, and the numbering therein will be used to structure the following discussion. From bulk thermodynamics, we would expect the system to evolve directly from fcc Au to two solid phases from the outset (Figure 2, process (1)), and the central question is why the liquid forms at all. If the temperature is sufficiently low, we might expect condensation of amorphous Ge, poisoning the

DOI: 10.1021/nl101349e | *Nano Lett.* **2010,** *10,* 2972--2976

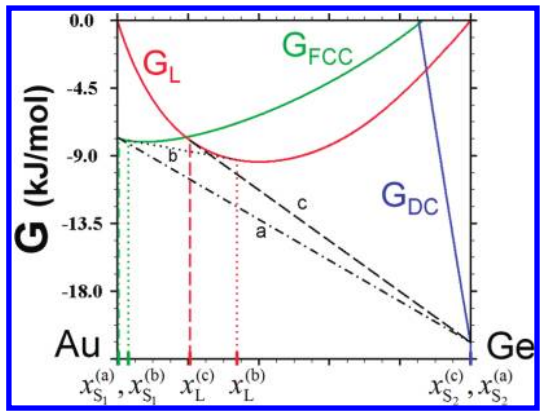

FIGURE 3. Calculated[26,27] free energies (G) and common tangents for the Au−Ge system at $T = 240$ °C. The free energies for the fcc, DC, and liquid (L) phases are represented in green, blue, and red, respectively. Tangent "a" corresponds to the Ge concentrations where fcc and DC are in equilibrium. Tangent "b" corresponds to the Ge concentrations where fcc and L are in equilibrium. Tangent "c" corresponds to the Ge concentrations where DC and L are in equilibrium. Ge concentrations at the tangent points are denoted by x, with the superscript indicating which tangent line and the subscript indicating which phase the concentration corresponds to. The calculated Ge equilibrium concentrations are as follows: $x_{S1}^{(a)} = 0.003$, $x_{S2}^{(a)} = 1.000$, $x_{S1}^{(b)} = 0.030$, $x_{L}^{(b)} = 0.338$, $x_{L}^{(c)} = 0.206$, and $x_{S2}^{(c)} = 1.000$.

fcc Au catalyst, Figure 2 process (3). However, even at 240 °C process (3) is not observed.

Our explanation of liquid formation involves the interplay between bulk thermodynamics and the kinetics of nucleation. Figure 3 shows the calculated free energy at 240 °C vs composition of the three relevant phases: fcc Au (with some dissolved Ge), liquid Au−Ge, and DC Ge (with negligible solubility of Au).[26,27] In equilibrium, as we add Ge to the Au, it should phase-separate into Au and Ge when the Ge concentration reaches $x_{S1}^{(a)} \approx 0.003$ as indicated by the common tangent between these phases (tangent "a" in Figure 3). However, it is well-known that nucleation of a new phase typically requires a significant supersaturation, and this is especially true for DC. If the composition of the fcc solid continues to rise without nucleation of DC Ge, then when the fcc solid reaches $x_{S1}^{(b)} \approx 0.03$ Ge (tangent "b" in Figure 3), it becomes thermodynamically favorable to form liquid Au−Ge, Figure 2 process 2.

A crucial point here is that, in contrast to DC Ge, we expect no nucleation barrier to forming the Au−Ge liquid, at least within a simple continuum picture of the nucleation process. In this textbook picture, the free energy of a particle of volume V of the new phase can be schematically written as

$$E = \beta V^{2/3} - (\Delta\mu)V \qquad (1)$$

where the coefficient β is a geometrically weighted difference of interfacial energies, reflecting the change in interfacial free energy associated with forming the new phase, and $\Delta\mu$ represents the bulk thermodynamic driving force.[28,29] For the nucleation of DC Ge from the Au−Ge liquid, $\Delta\mu$ is the chemical potential of Ge in the liquid, relative to DC Ge. The nucleation barrier E_B (thermal activation energy) is then given by the maximum of eq 1, i.e.

$$E_B \propto (\beta)^3/(\Delta\mu)^2 \qquad (2)$$

We see in Figure 1a that the liquid Au−Ge completely wets Au, consistent with what has been seen in Au−Si.[22] According to Young's equation, the absence of a finite wetting angle indicates that the excess interfacial energy is zero or negative, so $\beta \leq 0$ and no barrier is expected to forming the liquid phase. Thus, as Ge is deposited on the surface and diffuses into the Au, we expect liquid Au−Ge to form (Figure 2 process (2)) as soon as the Ge concentration in Au reaches the thermodynamic fcc−liquid transition ($x_{S1}^{(b)}$ in Figure 3).

In this picture, the only requirement for liquid formation and growth at 240 °C is the suppression of DC Ge nucleation. For temperatures slightly below the eutectic, $\Delta\mu$ is small along the fcc−liquid tangent line, so by eq 2 the barrier to nucleate DC Ge is prohibitively large. In that case liquid growth seems inevitable. At temperatures further below T_e $\Delta\mu$ increases. Figure 4a shows the evolution of the chemical potential at 240 °C, which can be directly compared with Figure 3. As Ge dissolves into the fcc Au, the Ge chemical potential rises sharply until the composition $x_{S1}^{(b)}$ is reached, at which point liquid Au−Ge forms. The supersaturation $\Delta\mu$ is substantial, but the large interfacial energy of DC Ge (giving large β) prevents nucleation of DC Ge from preempting the formation of the liquid. Then the chemical potential remains constant as Ge is added, due to the fcc−liquid coexistence. When the system composition reaches $x_{L}^{(b)}$, there is no more fcc phase (Figure 2 process (4)), and beyond this the chemical potential again rises as the liquid composition increases. Thus the barrier for nucleation of DC Ge decreases until nucleation occurs, Figure 2 process (6).

At 340 °C, slightly below T_e, Figure 4b shows that again $\Delta\mu > 0$ when the liquid forms, but $\Delta\mu$ is much smaller than at 240 °C, and it remains small until after the fcc Au has all dissolved, so according to eq 2, nucleation of DC Ge is far more strongly suppressed than at 240 °C. Above T_e (Figure 4c), the chemical potential remains below that of DC Ge (i.e., $\Delta\mu < 0$) until after the liquid has formed and the fcc Au has all dissolved.

Figure 1e shows that once Ge nucleates, the system rapidly separates into two solid phases with no liquid remaining. This is the thermodynamically expected process (7) of Figure 2. A Ge NW then grows as material is added in a layer-by-layer fashion at the solid Au−solid Ge interface,[11] Figure 2 process (9). Ge entering the solid catalyst will increase the chemical potential until, as we clearly can observe, a ledge nucleates and flows across the catalyst−Ge NW interface. A more detailed study of these interface

DOI: 10.1021/nl101349e | *Nano Lett.* **2010,** *10,* 2972–2976

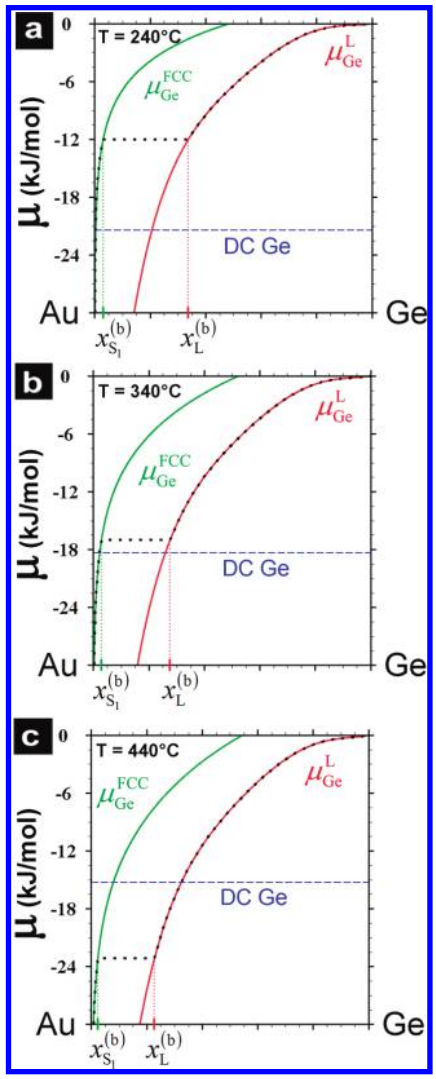

FIGURE 4. The chemical potentials for the fcc and liquid (L) phases at various temperatures. The green and the red curve represent fcc and L, respectively. The black dotted line represents the actual system evolution, with no DC Ge present; the horizontal crossover between the two curves corresponds to the fcc−liquid tangent "b" in Figure 3, and labels $x_{S_1}^{(b)}$ and $x_L^{(b)}$ in (a) refer to the same compositions as in Figure 3. The blue, dashed line indicates the chemical potential at which DC Ge would appear in thermodynamic equilibrium.

dynamics and supersaturation-dependent Au phases is beyond the scope of this paper and will be discussed elsewhere.

We find however that an alternative process can also occur—the catalyst can remain liquid after Ge precipitation, as in Figure 2 process (8). Panels a−c of Figure 5 show SiO_x supported Au nanoparticles, which after DC Ge nucleation remain in the liquid state at ∼240 °C in ∼0.9×10^{-3} mbar Ge_2H_6. Subsequent Ge NW growth appears to follow a VLS mechanism, Figure 5d, even though the temperature is more than 100 °C below T_e and has never been raised above T_e for the entire CVD process.

After Ge nucleation, excess Ge precipitates from the supersaturated liquid onto the new DC Ge nanowire. The level of Ge supersaturation then depends on the kinetics of

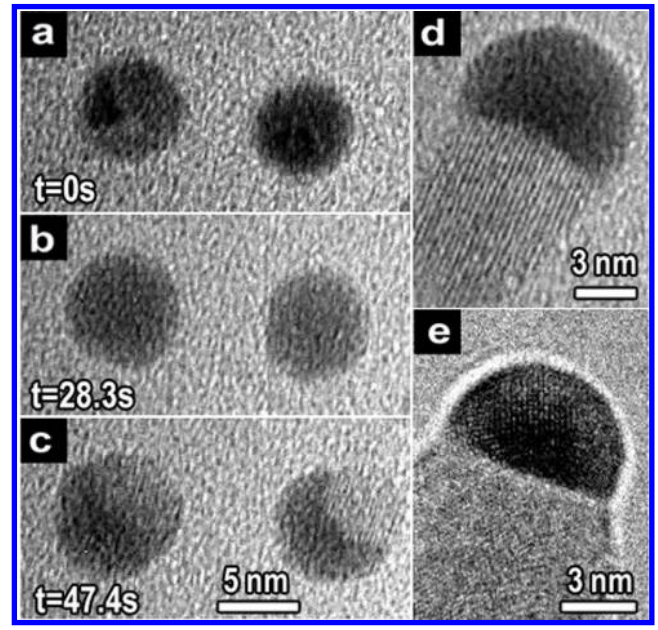

FIGURE 5. (a−c) Plan-view ETEM image sequence of SiO_x supported Au nanoparticles at ∼240 °C exposed to ∼0.9×10^{-3} mbar Ge_2H_6 (extracted from video S2, Supporting Information). ETEM image of Au at Ge NW tip at (d) ∼240 °C in ∼0.9×10^{-3} mbar Ge_2H_6 and at (e) ∼240 °C in ∼1.7×10^{-2} mbar Ge_2H_6 (30%)/He.

Ge addition to the liquid catalyst versus the Ge capture by the DC Ge crystal. A drop in Ge supersaturation causes the chemical potential of Au in the liquid to rise, which lowers the fcc nucleation barrier. We note that if the Ge concentration in the liquid remains above $x_L^{(b)}$ (Figure 3), it is unfavorable for fcc Au to form, regardless of its nucleation barrier. Hence a (significant) Ge supersaturation can cause the catalyst to remain liquid, as previously shown by undercooling for (nanoscale) Au−Ge.[4,5]

Within the probed conditions at 240 °C, we find the catalyst particles to solidify either immediately upon Ge nucleation (Figure 1) or after some initial VLS-like NW growth (and particle/NW coalescence), as in Figure 2 process (10), and eventually follow VSS-type growth, Figure 5e. Maintaining the liquid after Ge nucleation and VLS-like NW growth at higher growth rates appear more frequent at higher temperatures and digermane (partial) pressures, indicating how kinetically driven supersaturations determine the catalyst phase during NW CVD.

Our arguments have been simple and general, making no explicit assumptions about nanoscale size effects. Such effects could additionally contribute to stabilizing the liquid. In any case, we note that the large supersaturations at play here are not expected in truly macroscopic systems. A large system has a proportionally larger number of nucleation sites, with a high probability of including a preferred nucleation site such as an impurity. Such extrinsic size effects have been well studied in the past,[30] limiting the undercooling with increasing system size.

In conclusion, we have observed in situ the metastable liquefaction of sub-30-nm Au catalyst particles during diger-

DOI: 10.1021/nl101349e | *Nano Lett.* **2010,** *10,* 2972--2976

mane exposure at temperatures far below the bulk Au−Ge eutectic temperature. Upon Ge crystal nucleation and subsequent GeNW growth, the catalyst either recrystallizes or remains liquid, stabilized by the Ge supersaturation. We propose that at moderate supersaturation the diamond-cubic phase is kinetically inaccessible because of its high nucleation barrier, while the Au−Ge liquid is both kinetically accessible and thermodynamically favorable even at 240 °C. We believe that such metastable nanoparticle phases are relevant to other materials systems and of key importance to controlled bottom-up crystal growth and materials design for nanotechnology.

Acknowledgment. A.D.G. acknowledges funding from the Marshall Aid Commemoration Commission, and C.D. and S.H. acknowledge funding from the Royal Society.

Supporting Information Available. ETEM videos (.avi, corresponding to Figures 1 and 5) and descriptive text (.pdf) of SiO_x supported Au nanoparticles during Ge_2H_6 exposure at ~240 °C. This material is available free of charge via the Internet at http://pubs.acs.org.

REFERENCES AND NOTES

(1) Hiruma, K.; Yazawa, M.; Katsuyama, T.; Ogawa, K.; Haraguchi, K.; Koguchi, M.; Kakibayashi, H. *J. Appl. Phys.* **1995**, *77*, 447.
(2) Li, Y.; Qian, F.; Xiang, J.; Lieber, C. M. *Mater. Today* **2006**, *9*, 18.
(3) Fan, H. J.; Werner, P.; Zacharias, M. *Small* **2006**, *2*, 700.
(4) Kodambaka, S.; Tersoff, J.; Reuter, M. C.; Ross, F. M. *Science* **2007**, *316*, 729.
(5) Adhikari, H.; Marshall, A. F.; Goldthorpe, I. A.; Chidsey, C. E. D.; McIntyre, P. C. *ACS Nano* **2007**, *1*, 415.
(6) Wang, Y. W.; Schmidt, V.; Senz, S.; Gosele, U. *Nat. Nanotechnol.* **2006**, *1*, 186.
(7) Wacaser, B. A.; Reuter, M. C.; Khayyat, M. M.; Wen, C. Y.; Haight, R.; Guha, S.; Ross, F. M. *Nano Lett.* **2009**, *9*, 3296.
(8) Persson, A. I.; Larsson, M. W.; Stenstrom, S.; Ohlsson, B. J.; Samuelson, L.; Wallenberg, L. R. *Nat. Mater.* **2004**, *3*, 677.
(9) Harmand, J. C.; Patriarche, G.; Pere-Laperne, N.; Merat-Combes, M. N.; Travers, L.; Glas, F. *Appl. Phys. Lett.* **2005**, *87*, 3.
(10) Wen, C. Y.; Reuter, M. C.; Bruley, J.; Tersoff, J.; Kodambaka, S.; Stach, E. A.; Ross, F. M. *Science* **2009**, *326*, 1247.
(11) Hofmann, S.; Sharma, R.; Wirth, C. T.; Cervantes-Sodi, F.; Ducati, C.; Kasama, T.; Dunin-Borkowski, R. E.; Drucker, J.; Bennett, P.; Robertson, J. *Nat. Mater.* **2008**, *7*, 372.
(12) Bootsma, G. A.; Gassen, H. J. *J. Cryst. Growth* **1971**, *10*, 223.
(13) Miyamoto, Y.; Hirata, M. *Jpn. J. Appl. Phys.* **1975**, *14*, 1419.
(14) Wang, D.; Dai, H. *Angew. Chem., Int. Ed.* **2002**, *41*, 4783.
(15) Greytak, A. B.; Lauhon, L. J.; Gudiksen, M. S.; Lieber, C. M. *Appl. Phys. Lett.* **2004**, *84*, 4176.
(16) Adhikari, H.; McIntyre, P. C.; Marshall, A. F.; Chidsey, C. E. D. *J. Appl. Phys.* **2007**, *102*, No. 094311.
(17) Li, C. B.; Usami, K.; Muraki, T.; Mizuta, H.; Oda, S. *Appl. Phys. Lett.* **2008**, *93*, No. 041917.
(18) Varahramyan, K. M.; Ferrer, D.; Tutuc, E.; Banerjee, S. K. *Appl. Phys. Lett.* **2009**, *95*, 3.
(19) Sierra-Sastre, Y.; Dayeh, S. A.; Picraux, S. T.; Batt, C. A. *ACS Nano* **2010**, *4*, 1209.
(20) Weissmüller, J.; Bunzel, P.; Wilde, G. *Scr. Mater.* **2004**, *51*, 813.
(21) Schwalbach, E. J.; Voorhees, P. W. *Nano Lett.* **2008**, *8*, 3739.
(22) Kim, J.; Tersoff, J.; Wen, C. Y.; Reuter, M. C.; Stach, E. A.; Ross, F. M. *Phys. Rev. Lett.* **2009**, *103*, 155701.
(23) Utke, I.; Hoffmann, P.; Melngailis, J. *J. Vac. Sci. Technol., B* **2008**, *26*, 1197.
(24) In particular for reduced digermane pressures and high magnifications (i.e., high e^- impingement flux), we observe Ge NW/film nucleation to be preferential/faster within the e-beam exposed area. We expect this to be mainly due to e-beam induced digermane dissociation (see ref 23), which increases the Ge supersaturation. We think the observed e-beam effects do not affect the general validity of the observed growth phenomena, in particular as an increase of the digermane pressure accelerates GeNW growth over the whole (also non-e-beam exposed) sample area.
(25) Koga, K.; Ikeshoji, T.; Sugawara, K.-I. *Phys. Rev. Lett.* **2004**, *92*, 115507.
(26) Chevalier, P. Y. *Thermochim. Acta* **1989**, *141*, 217.
(27) Almazouzi, A.; Bernardini, J.; Moya, E. G.; Bracht, H.; Stolwijk, N. A.; Mehrer, H. *J. Appl. Phys.* **1991**, *70*, 1345.
(28) Turnbull, D.; Fisher, J. C. *J. Chem. Phys.* **1949**, *17*, 71.
(29) Porter, D. A.; Easterling, K. E.; Sherif, M. Y. *Phase Transformations in Metals and Alloys*; CRC Press: Boca Raton, FL, 2009.
(30) Takahashi, T.; Tiller, W. A. *Acta Metall.* **1969**, *17*, 643.

DOI: 10.1021/nl101349e | *Nano Lett.* **2010,** *10,* 2972--2976